Master's Thesis Presentation for the 142th Dissertation Evaluation

A Study on Posterior Extraocular Muscles Segmentation in CT Image of Dysthyroid Optic Neuropathy Patients

갑상선 시신경병증 CT 이미지 분석을 위한 후방 외안근 세그멘테이션에 관한 연구

Mingi Kim

ddmr0608@gmail.com

13th Nov, 2024

Contents

Introduction

Thyroid-Associated Ophthalmopathy and Dysthyroid Optic Neuropathy

- Thyroid-Associated Ophthalmopathy (TAO), an autoimmune eye condition associated with thyroid dysfunction, is characterized by the presence of deformation in the extraocular muscles, which can lead to diseases such as Dysthyroid Optic Neuropathy (DON) [1,2,3].
- DON, a complication of TAO where early diagnosis is important, involves swelling of the Extraocular muscles and Orbital fatty connective tissue, leading to optic nerve compression and subsequent loss of the Retinal Nerve Fiber Layer (RNFL) [3,4].

TAO & DON patient's images

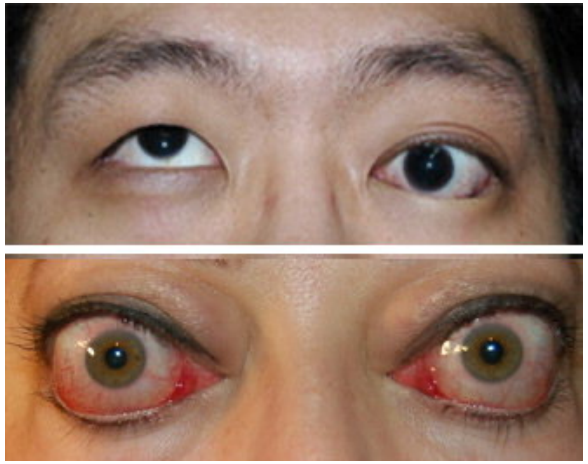

Fig. (a) TAO patients

Fig. (b) DON patients

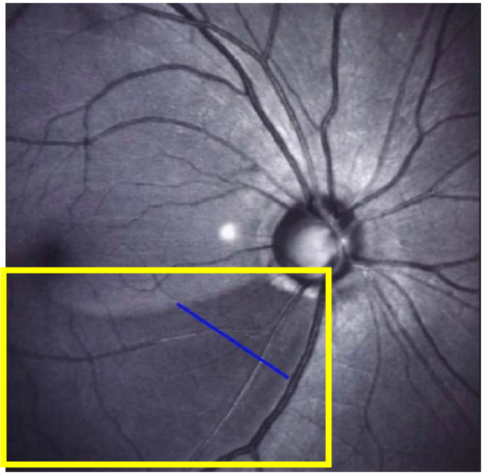

Fig. (c) DON patient's RNFL impairment

[1] Huang et al. "The significance of ophthalmological features in diagnosis of thyroid-associated ophthalmopathy." BioMedical Engineering OnLine 22.1 (2023): 7.
[2] Rana et al. "Extraocular muscle enlargement in dysthyroid optic neuropathy." Canadian Journal of Ophthalmology (2023).
[3] Tu et al. "Modified endoscopic transnasal orbital apex decompression in dysthyroid optic neuropathy." *Eye and Vision* 8.1 (2021): 19.
[4] Luo et al. "Retinal nerve fiber layer and ganglion cell complex thickness as a diagnostic tool in early stage dysthyroid optic neuropathy." *European Journal of Ophthalmology* 32.5 (2022): 3082-3091.

Introduction

Compression of the Optic nerve

- Symptoms of Optic nerve compression, including decreased visual acuity, visual field defects, and abnormal color vision, can be identified with ocular imaging technology, but definitive diagnosis requires radiologists' expertise, emphasizing the need for prompt treatment [5].
- DON-induced Optic nerve compression is primarily influenced by volumetric expansion of the posterior part of the Extraocular muscles at Orbital apex, and various treatment methods such as Ophthalmic decompression are performed [3,5,6].

Axial view of the Optic nerve & Extraocular muscles

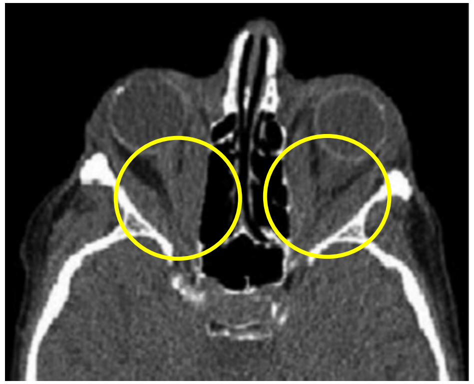

Fig. (a) Optic nerve compression from a swollen Extraocular muscles

Fig. (b) Normal Optic nerve & Extraocular muscles

Orbital tissues in Orbital apex

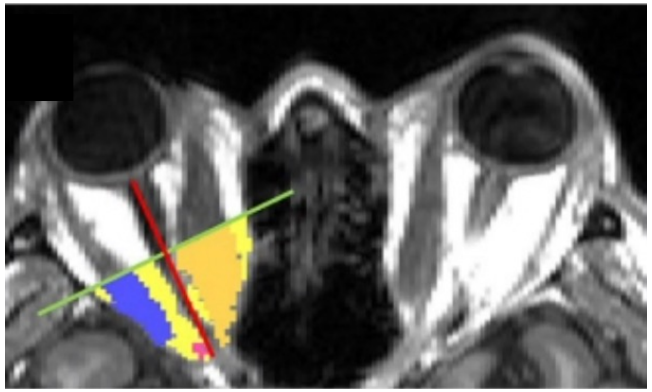

Fig. (c) Orbital tissues in Orbital apex

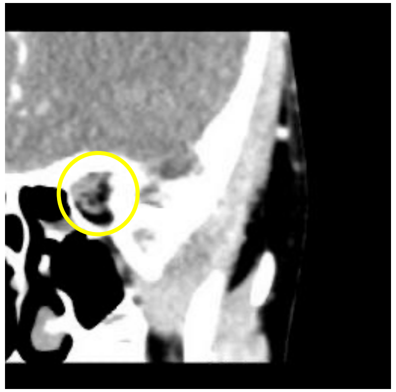

Fig. (d) Extraocular muscles in Orbital apex

[3] Tu et al. "Modified endoscopic transnasal orbital apex decompression in dysthyroid optic neuropathy." *Eye and Vision* 8.1 (2021): 19.
[5] Song et al. "Extraocular muscle volume index at the orbital apex with optic neuritis: a combined parameter for diagnosis of dysthyroid optic neuropathy." European Radiology 33.12 (2023): 9203-9212.
[6] Rootman et al. "Orbital decompression for thyroid eye disease." Survey of Ophthalmology 63.1 (2018): 86-104.

Introduction

Objectives and Standard Procedure

- We aim to provide sophisticated segmentation masks for the Posterior Extraocular muscles of the Orbital apex, with the obtained masks also usable for volume measurement to disease detection and treatment planning in DON diagnosis [3,5,7].
- Using Computed Tomography (CT) images of the Posterior Extraocular muscles at the orbital apex as input data, the neural network for segmentation outputs masks that identify structurally significant regions of the target muscles.

Coronal view CT images of the extraocular muscles

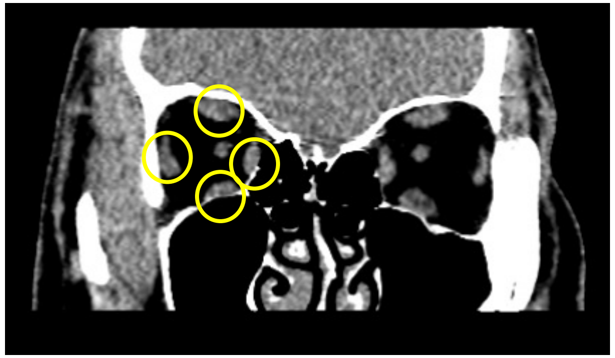

Fig. (a) Extraocular muscles

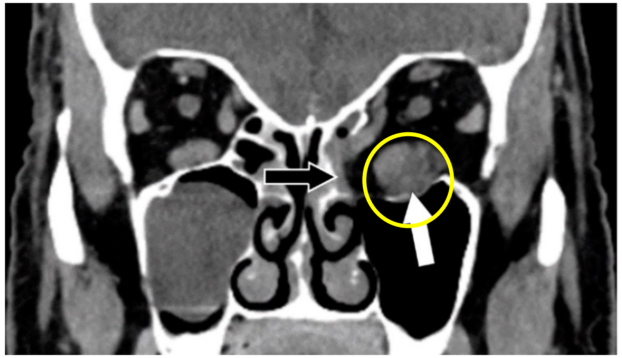

Fig. (b) CT image of swollen Inferior Rectus (Part of Extraocular muscles)

Overview of segmentation procedure based on neural networks

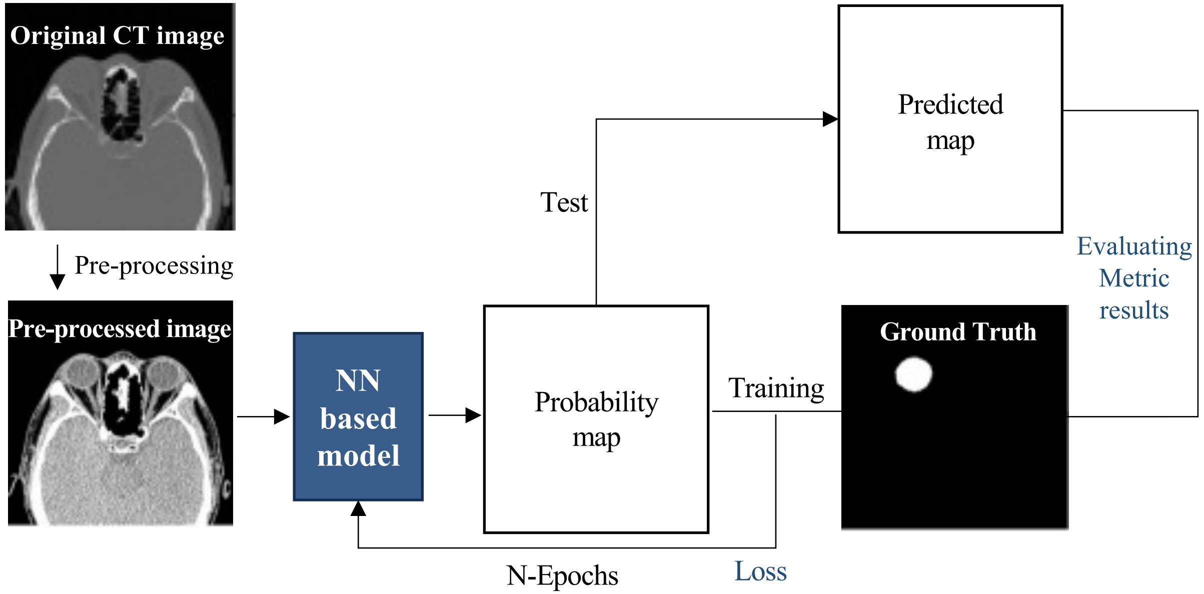

[3] Tu et al. "Modified endoscopic transnasal orbital apex decompression in dysthyroid optic neuropathy." *Eye and Vision* 8.1 (2021): 19.
[5] Song et al. "Extraocular muscle volume index at the orbital apex with optic neuritis: a combined parameter for diagnosis of dysthyroid optic neuropathy." European Radiology 33.12 (2023): 9203-9212.
[7] Diao et al. "Research progress and application of artificial intelligence in thyroid associated ophthalmopathy." *Frontiers in Cell and Developmental Biology* 11 (2023): 1124775.

Introduction

Problem and Strategy

- The Orbital apex, where the Posterior Extraocular muscles are located, has a complex structure that is difficult to distinguish from each other due to the small size of the tissues, making it difficult to learn neural networks for identifying Optic nerve compression [5].
- Accurately segmenting small-sized tissues requires an encoding process that properly preserves and effectively extracts features from small receptive fields, particularly low-level semantic information such as edges.

Coronal view CT images of Inferior Rectus of the Orbital apex by patient

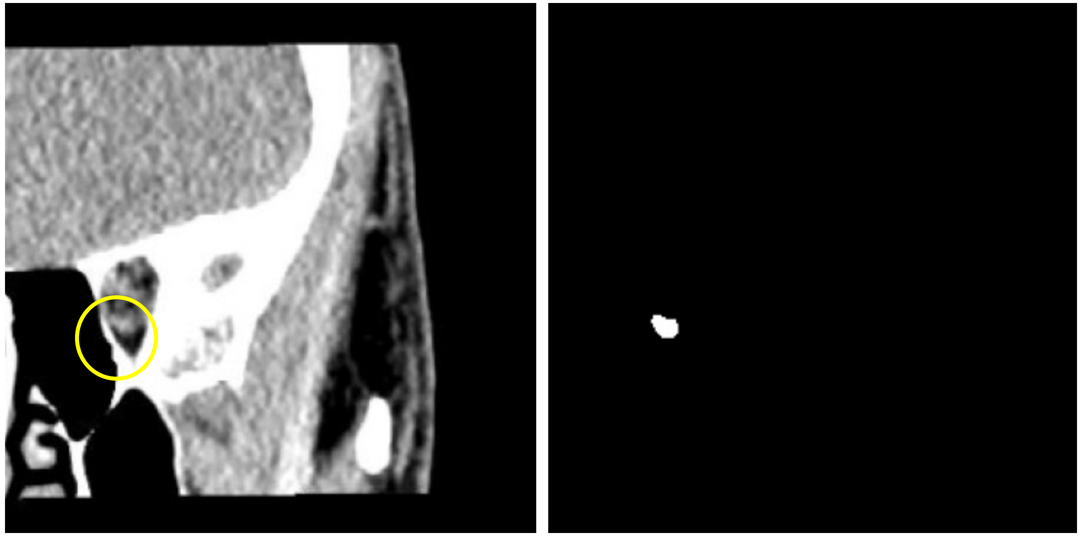

Fig. (a) Original image & Ground Truth of Patient 102

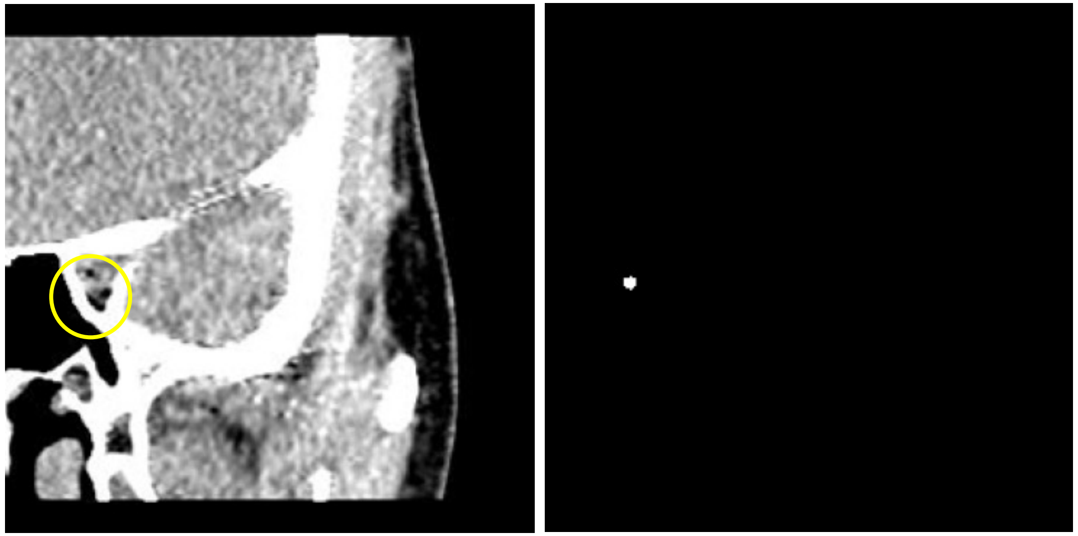

Fig. (b) Original image & Ground Truth of Patient 10102

[5] Song et al. "Extraocular muscle volume index at the orbital apex with optic neuritis: a combined parameter for diagnosis of dysthyroid optic neuropathy." European Radiology 33.12 (2023): 9203-9212.

Related Work

Medical Image Segmentation

- Medical image segmentation involves the precise, pixel-level identification of specific organs, inflamed areas, or tissue regions in medical images, including MRI and CT scans. Research in this field has significantly advanced medical diagnosis and treatment [8].
- Recently, neural networks (NNs) have been widely applied in medical diagnosis, with most studies employing Convolutional Neural Networks (CNNs) due to their strengths in local feature extraction, a crucial aspect in the medical field [9].

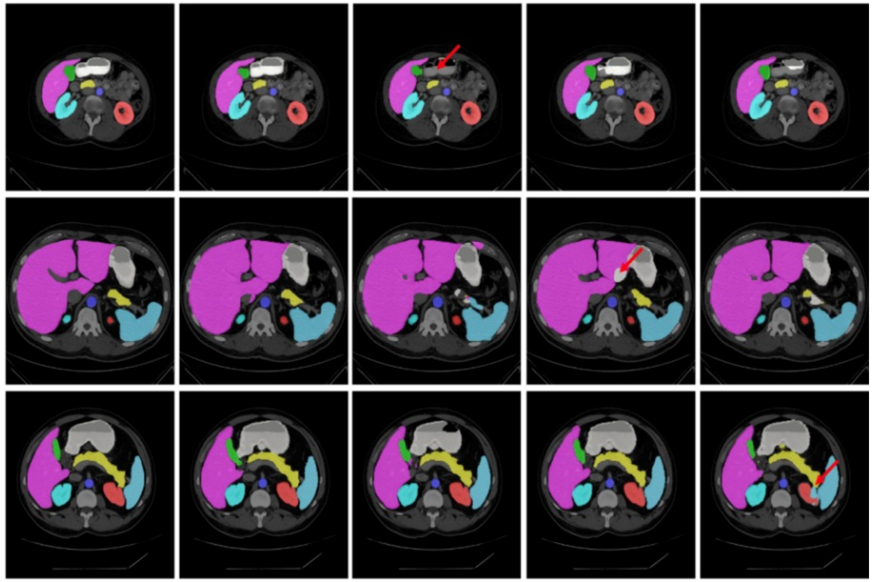

Synapse multi-organ CT

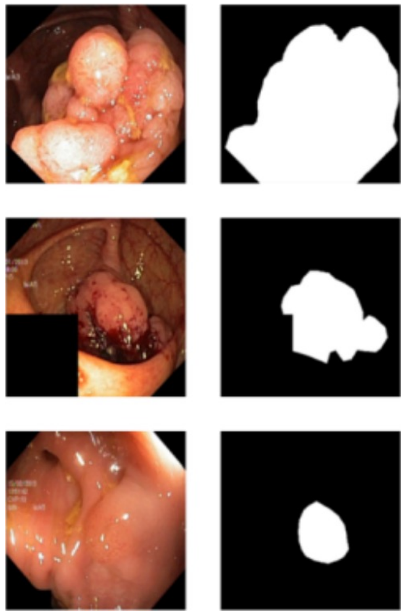

Kvasir-SEG

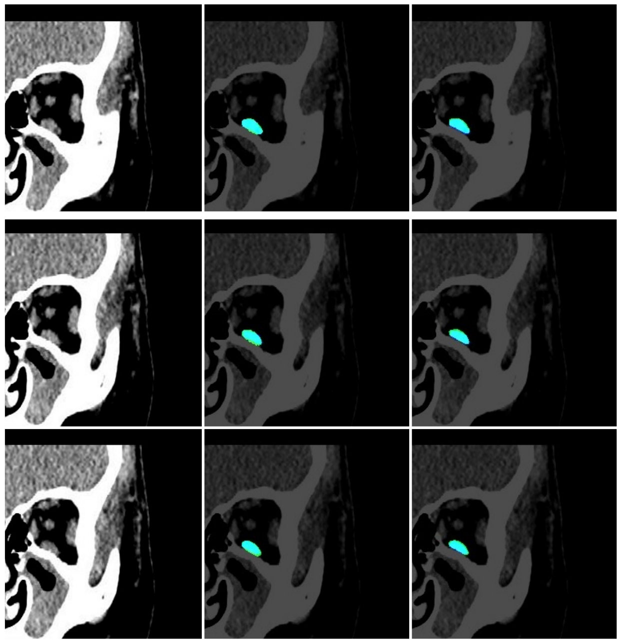

Extraocular muscles CT

[8] Wang et al. "Medical image segmentation using deep learning: A survey." IET image processing 16.5 (2022): 1243-1267.
[9] Yuan et al. "An effective CNN and Transformer complementary network for medical image segmentation." Pattern Recognition 136 (2023): 109228.

Related Work

Meganet: Multi-scale edge-guided attention network for weak boundary polyp segmentation

- MEGANet outperforms other state-of-the-art methods in polyp segmentation on several benchmark datasets through both qualitative and quantitative evaluations. It combines edge detection and attention mechanisms to effectively preserve polyp boundaries.
- Due to the limited feature extraction capabilities of tiny receptive fields for segmenting small objects, this study is not effective in the Posterior Extraocular muscles of the Orbital apex, which is small in size and has unclear boundaries.

Illustration of the model

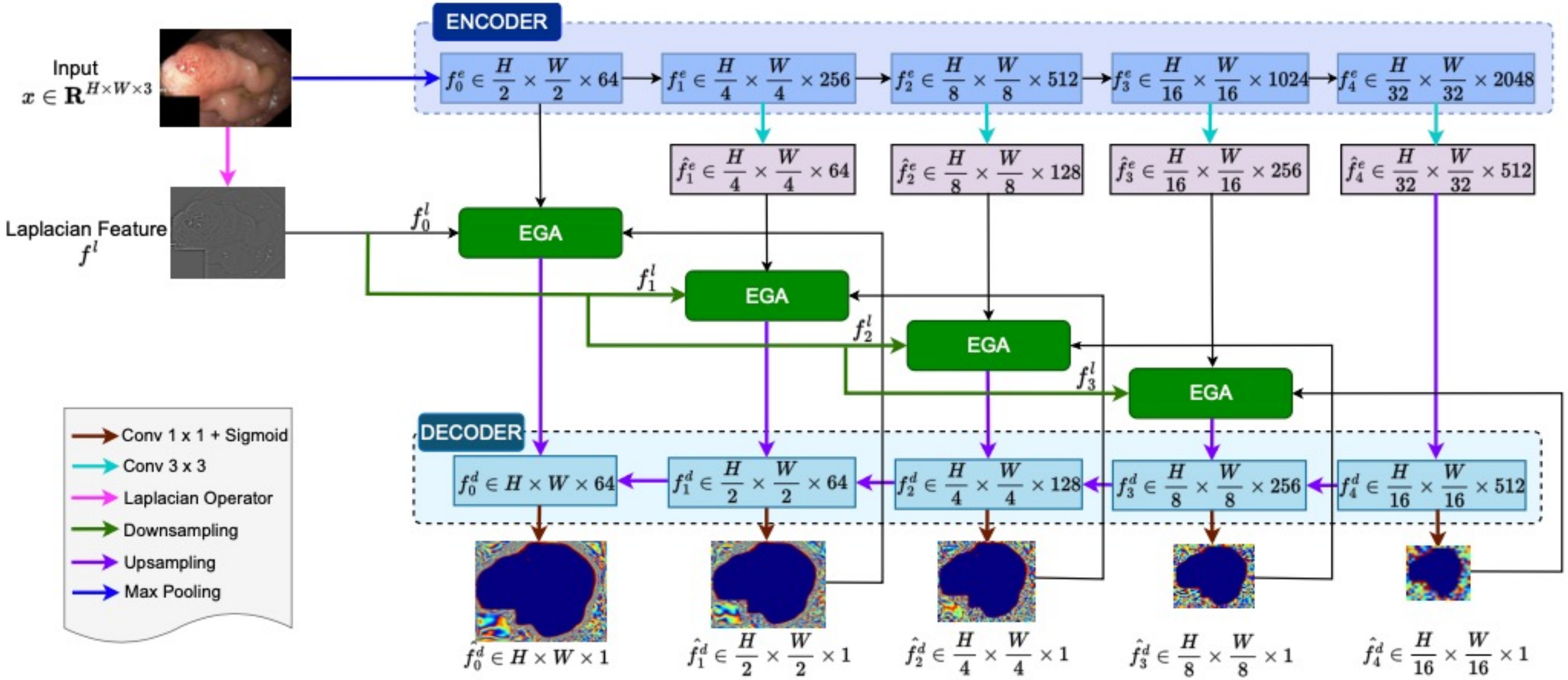

[10] Bui et al. "Meganet: Multi-scale edge-guided attention network for weak boundary polyp segmentation." Proceedings of the IEEE/CVF Winter Conference on Applications of Computer Vision. 2024.

Related Work

Levit-unet: Make faster encoders with transformer for medical image segmentation

- Using LeViT as the encoder, LeViT-UNet achieves superior performance on challenging medical image segmentation benchmarks by integrating a LeViT Transformer module with the U-Net architecture.
- Due to the limited feature extraction capabilities of tiny receptive fields for segmenting small objects, this study is not effective in the Posterior Extraocular muscles of the Orbital apex, which is small in size and has unclear boundaries.

Illustration of the model

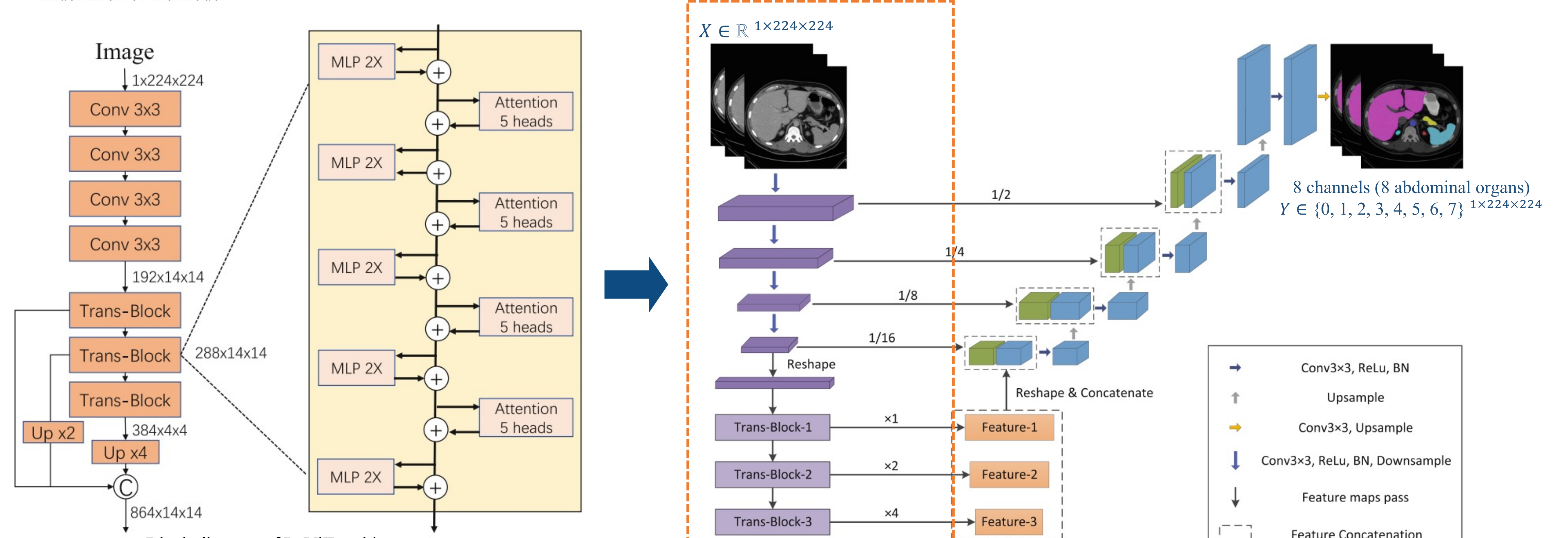

Block diagram of LeViT architecture

[11] Xu et al. "Levit-unet: Make faster encoders with transformer for medical image segmentation." Chinese Conference on Pattern Recognition and Computer Vision (PRCV). Singapore: Springer Nature Singapore, 2023.

Related Work

Using DUCK-Net for polyp image segmentation

- DUCKNet achieves state-of-the-art results in polyp segmentation on benchmark datasets. The model utilizes an encoder-decoder structure with residual downsampling and custom convolutional blocks to effectively process image information.
- Due to the limited feature extraction capabilities of tiny receptive fields for segmenting small objects, this study is not effective in the Posterior Extraocular muscles of the Orbital apex, which is small in size and has unclear boundaries.

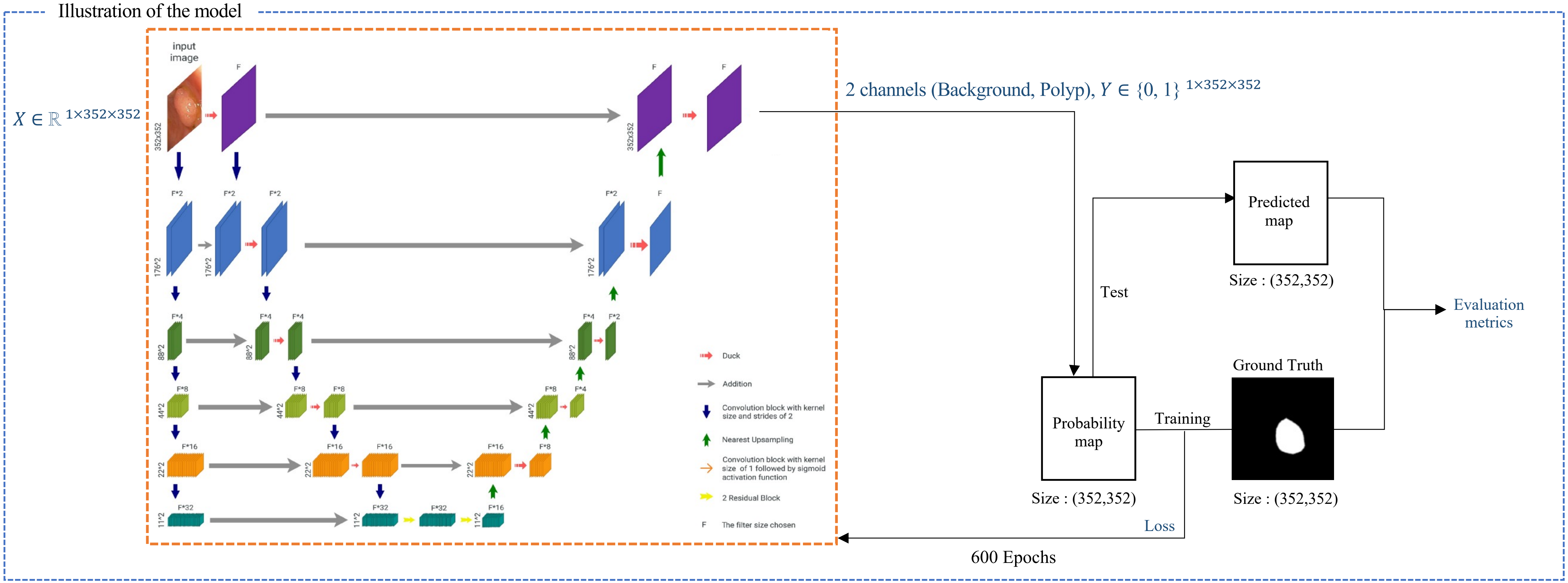

[12] Dumitru et al. "Using DUCK-Net for polyp image segmentation." Scientific reports 13.1 (2023): 9803.

Related Work

Common Drawback and Solution

- Due to the limited feature extraction capabilities of tiny receptive fields for segmenting small objects, this study is not effective in the Posterior Extraocular muscles of the Orbital apex, which is small in size and has unclear boundaries.
- In this study, 1×1 convolution-enhanced first layer of the encoder and narrow receiving field features are effectively fused with large receiving field features to effectively extract features from small receiving fields during the entire encoding process.

Model	Author	Publication	Summary	Drawback
MEGANet	Bui et al. (2024)	IEEE/CVF Winter Conference on Applications of Computer Vision	MEGANet outperforms other state-of-the-art methods in polyp segmentation on five benchmark datasets through both qualitative and quantitative evaluations. The network combines edge detection and attention mechanisms to effectively preserve polyp boundaries in colonoscopy images.	Due to the limited feature extraction capabilities of tiny receptive fields for segmenting small objects, this study is not effective in the Posterior Extraocular muscles of the Orbital apex, which is small in size and has unclear boundaries.
LeViT-UNet	Xu et al. (2023)	Chinese Conference on Pattern Recognition and Computer Vision (PRCV)	LeViT-UNet achieves superior performance on challenging medical image segmentation benchmarks, by integrating a LeViT Transformer module with the U-Net architecture. This model balances accuracy and efficiency by using LeViT as the encoder and incorporating multi-scale feature maps via skip connections.	
DUCKNet	Dumitru et al. (2023)	Scientific reports	DUCKNet achieves state-of-the-art results in polyp segmentation on benchmark datasets, demonstrating excellent performance with limited training data. The model utilizes an encoder-decoder structure with residual downsampling and custom convolutional blocks to effectively process image information.	

[10] Bui et al. "Meganet: Multi-scale edge-guided attention network for weak boundary polyp segmentation." Proceedings of the IEEE/CVF Winter Conference on Applications of Computer Vision. 2024.
[11] Xu et al. "Levit-unet: Make faster encoders with transformer for medical image segmentation." Chinese Conference on Pattern Recognition and Computer Vision (PRCV). Singapore: Springer Nature Singapore, 2023.
[12] Dumitru et al. "Using DUCK-Net for polyp image segmentation." Scientific reports 13.1 (2023): 9803.

Proposed Method

Notation and Definition

- Given input, $X = \{X_i\}_{i=1}^{m}$ and their corresponding Ground Truth (GT) $Y = \{Y_i\}_{i=1}^{m}$, consider a 2D image $X_i \in R^{H\times W}$ with its associated GT C-class segmentation masks, $Y_i \in \{1,2,\dots,C\}^{H\times W}$, where H, W are height and width.
- The goal of segmentation is to design a function P so that $\widehat{Y_i} = P(X_i)$ is close to Y_i, with the parameters θ_P of P that are learned to minimize the segmentation loss $L = \sum_c (1 - TI_c)^{1/\gamma}$ over the entire dataset.

Notation	Name	Definition
$X = \{X_i\}_{i=1}^{m},\ X_i \in R^{H\times W}$	Input images	CT images of TAO patients as input
$Y = \{Y_i\}_{i=1}^{m},\ Y_i \in \{1,2,\dots,C\}^{H\times W}$	Ground Truth	Ground Truth of the Input images
$TI_c = \frac{\sum_{i=1}^{N} p_{ic} g_{ic} + \varepsilon}{\sum_{i=1}^{N} p_{ic} g_{ic} + \alpha \sum_{i=1}^{N} p_{i\bar{c}} g_{ic} + \beta \sum_{i=1}^{N} p_{ic} g_{i\bar{c}} + \varepsilon}$ $FTL_c = \sum_c (1 - TI_c)^{1/\gamma}$ where, p_{ic} is the probability that pixel i is of the lesion class c and p_{ic} is the probability pixel i is of the non-lesion class, $\bar{c}$. The same is true for g_{ic} and g_{ic}, respectively. α and β are hyper-parameters.	Focal Tversky Loss	Focal loss function based on the Tversky index to address the issue of data imbalance

Proposed Method

Procedural Overview

- In the CT original images of 205 TAO patients, a 256 × 256 near-end slice corresponding to the Posterior Extraocular muscles of the Orbital apex was selected and used as input data where the boundaries of the Extraocular muscles became unclear.
- The pre-processed data is input into the proposed encoder-decoder-based neural network model for training and optimization using Focal -Tversky loss, with performance measured using IoU, Dice-Coefficient, F1 score, Precision and Recall metrics on the evaluation dataset.

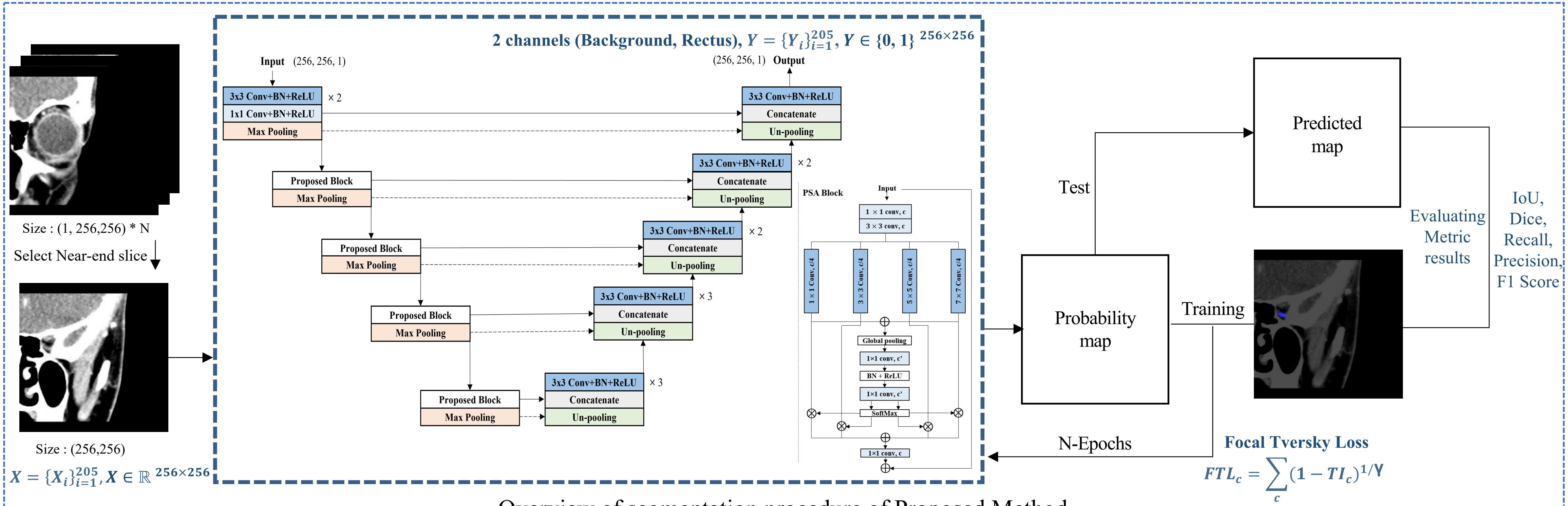

Overview of segmentation procedure of Proposed Method

Proposed Method

Proposed network architecture

- The first layer of the encoder is enhanced by 1×1 kernels, which help it extract spatial information of small receptive field effectively, which is essential for segmenting tiny object, from a high-resolution level feature map.
- Then, Proposed Split-Attention based block enhances multi receptive field information based on hierarchical convolution layers and split attention block by effectively fusing narrow receptive field feature and large receptive field feature.

Schematic overview of proposed encoder-decoder

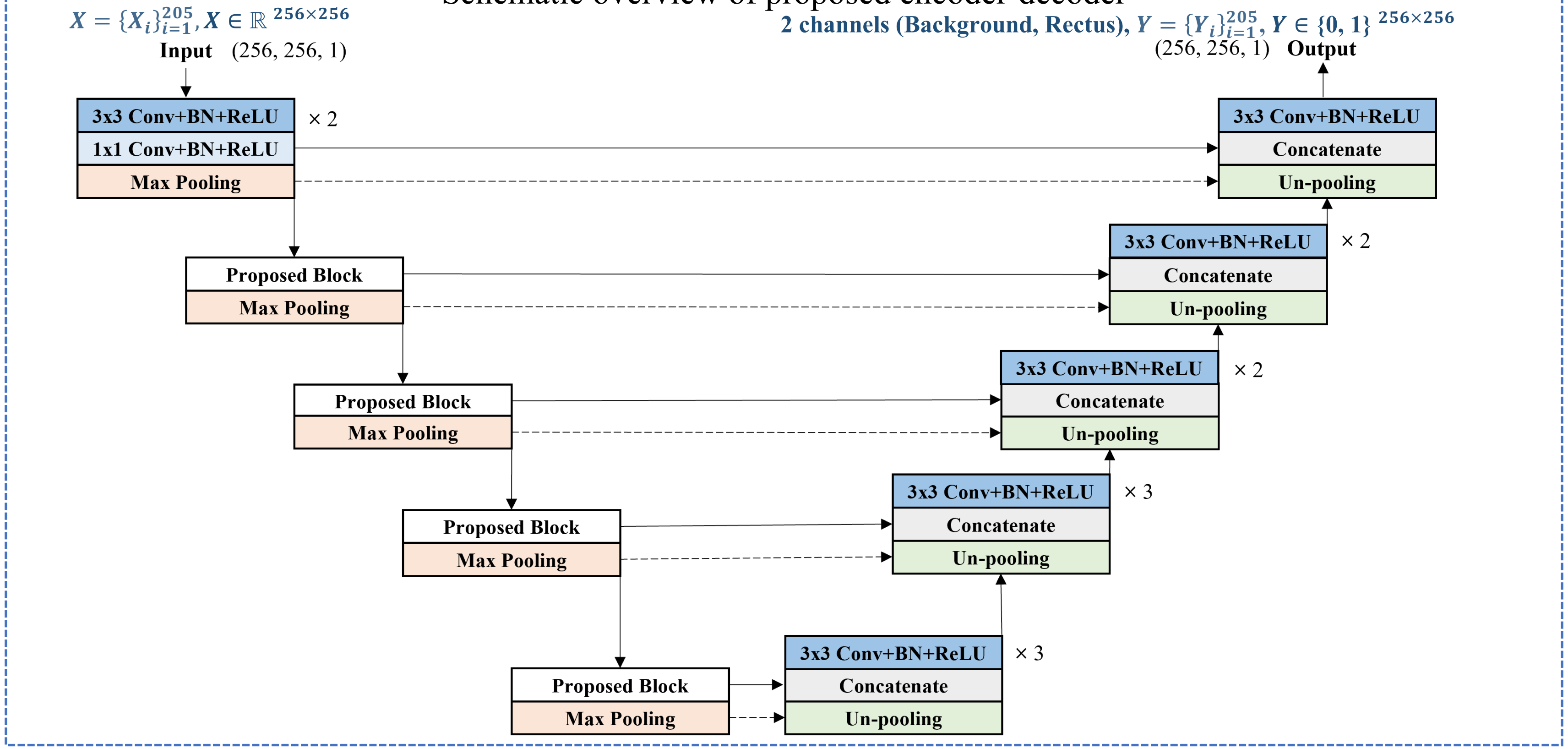

Proposed Method

Cross-Channel Feature Extraction

First layer of the encoder

- Given the small size and lack of clear boundaries in the Posterior Extraocular muscles image of the Orbital apex, we reinforced the first layer of the encoder to the extraction of low-level semantic information with high resolution features and edge information.
- By stacking the appropriate amount of convolutional layers, we added 1×1 convolutional layers following two 3×3 convolutional layers to avoid both overfitting through overly deep layers and underfitting through overly shallow layers.

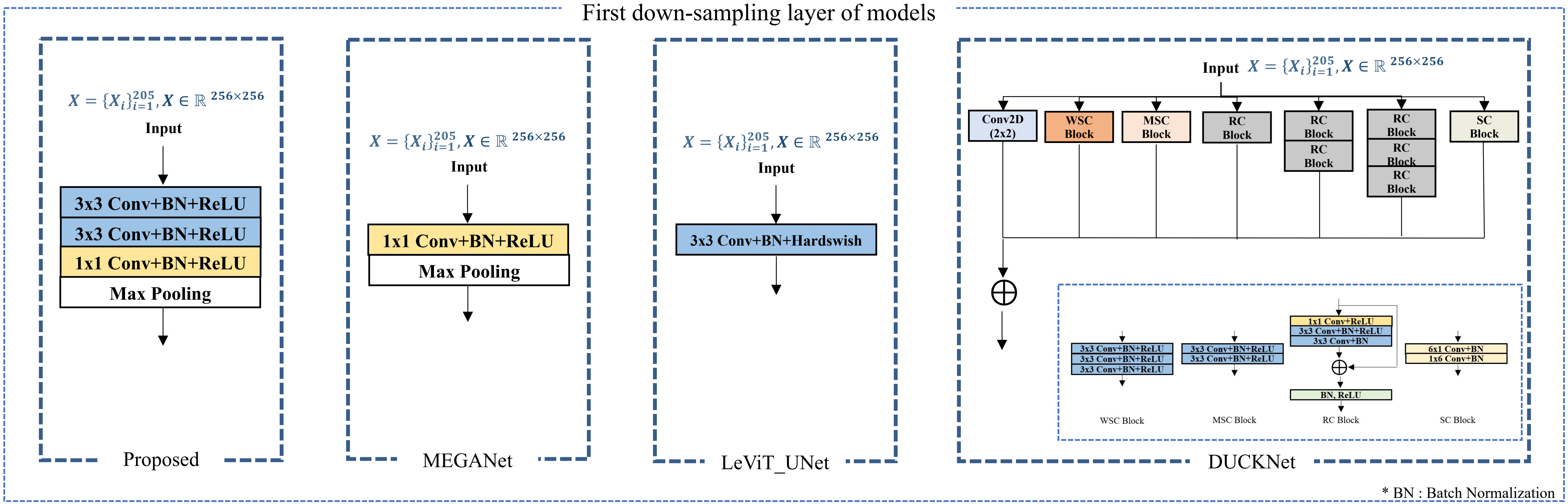

Proposed Method

Cross-Channel Feature Extraction

Proposed Split-Attention based block

- The Proposed block extracts base features using 1×1 and 3×3 convolution layers to make features suitable for conversion into pyramid features, and exploits convolution layers of different scales (i.e., 1×1, 3×3, 5×5, and 7×7) to create features with different receptive fields.
- Subsequently, the split-attention block [13] calculates channel scores for each feature split, assigns them after evaluating different scales, and aggregates the recalibrated features using channel-wise summation followed by a 1×1 convolution for final fusion.

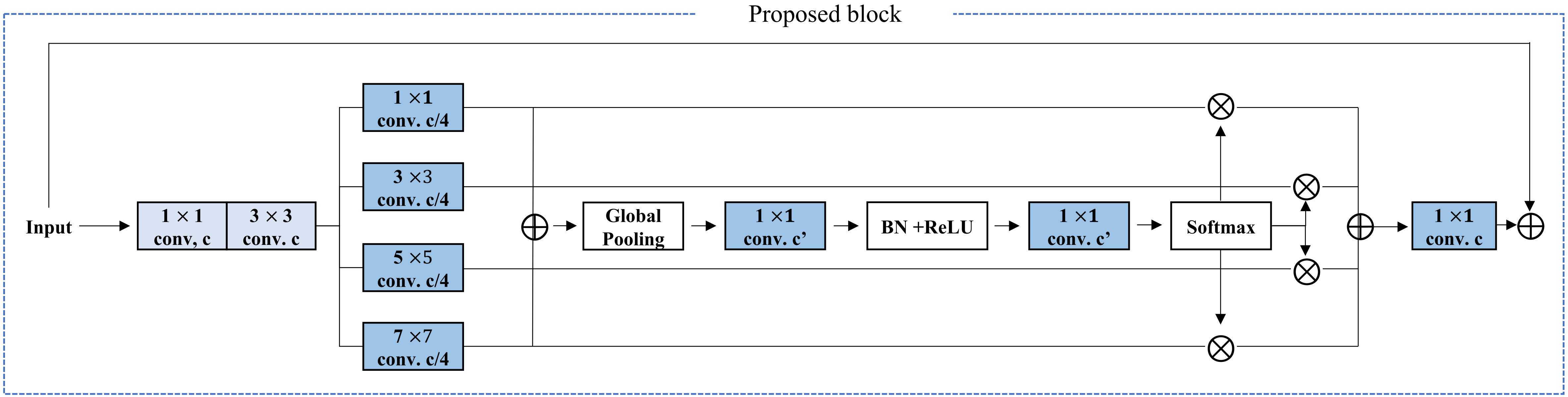

[13] Zhang et al. "ResNeSt: Split-Attention Networks." in *Proceedings of the IEEE/CVF Conference on Computer Vision and Pattern Recognition* 2022.

Experimental Settings

Data description

- Original dataset were obtained through CT images of 205 TAO patients and its Ground Truth was produced by manual annotation.

- Demographic statistics

Age (years, range)	Sex		Total (n, %)
	Male (n, %)	**Female (n, %)**	
59 and under	14 (6.8)	25 (12.2)	39 (19)
60-69	6 (2.9)	19 (9.3)	25 (12.2)
70-79	6 (2.9)	31 (15.1)	37 (18)
80-89	12 (5.9)	52 (25.4)	64 (31.2)
90 and over	9 (4.4)	31 (15.1)	40 (20)
Total	47 (22.9)	158 (77.1)	205

Dataset

- Each near-end slice from the Original dataset, where the boundaries of the Posterior Extraocular muscles are unclear, was used as input.

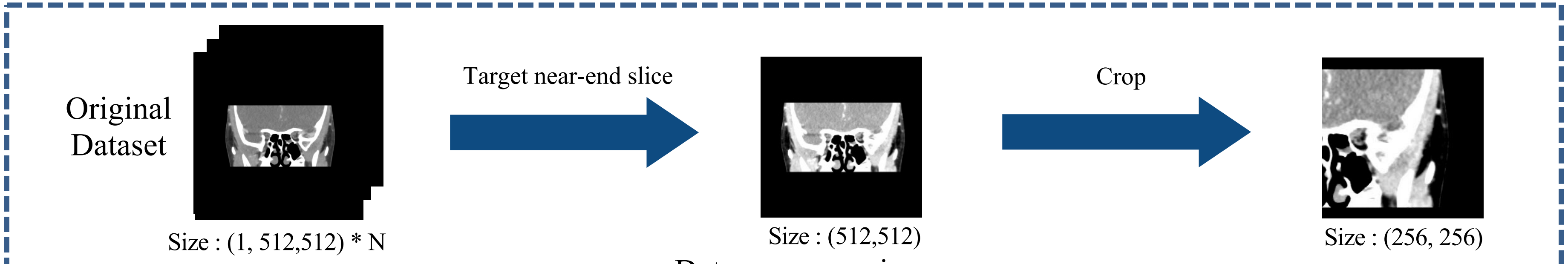

Data preprocessing process

Cross Validation

- Number of Iterations: 10

- Data Split Ratio (Train: Validation: Test) = 0.7 : 0.15: 0.15

Experimental Settings

Hyperparameter Settings

Model	Batch size	Epochs	Loss Function	Opimizer	Learning Rate
Proposed Model Bui et al. (2024) Xu et al. (2023) Dumitru et al. (2023)	8	125	Focal Tversky Loss	AdamW	1e-3 to 1e-6 by cosine annealing scheduler

Evaluation Measures

- $Dice\ coefficient = \frac{2TP}{2TP+FP+FN}$, $IoU(Intersection\ of\ Union) = \frac{TP}{TP+FP+FN}$, $F1\ Score = 2 \cdot \frac{Precision \cdot Recall}{Precision+Recall}$, $Precision = \frac{TP}{TP+FP}$, $Recall = \frac{TP}{TP+FN}$ are the evaluation metrics, where TP is true positive, FN is False Negative, TN is True Negative, and FP is False Positive.
- Paired t-test was conducted to verify the statistical significance of the evaluation metrics.

[10] Bui et al. "Meganet: Multi-scale edge-guided attention network for weak boundary polyp segmentation." Proceedings of the IEEE/CVF Winter Conference on Applications of Computer Vision. 2024.
[11] Xu et al. "Levit-unet: Make faster encoders with transformer for medical image segmentation." Chinese Conference on Pattern Recognition and Computer Vision (PRCV). Singapore: Springer Nature Singapore, 2023.
[12] Dumitru et al. "Using DUCK-Net for polyp image segmentation." Scientific reports 13.1 (2023): 9803.

Experimental Results

Comparison to Conventional Methods

- The proposed model, which focuses on effectively extracting features of tiny receptive fields, shows better performance in Dice Coefficient, IoU, Precision, and F1 Score compared to comparative models.

The asterisk (*) indicates statistical significance with all comparison models at the 0.01 level.

Model	Dice	p-value	IoU	p-value	Recall	p-value	Precision	p-value	F1 Score	p-value
Proposed	**0.766 ± 0.027***		**0.641 ± 0.026***		0.820 ± 0.046		**0.767 ± 0.040**		**0.766 ± 0.027***	
MEGANet	0.701 ± 0.044	< 0.005	0.573 ± 0.042	< 0.005	0.763 ± 0.052	0.094	0.721 ± 0.066	0.052	0.701 ± 0.044	< 0.005
LeViT-UNet	0.643 ± 0.036	< 0.005	0.509 ± 0.030	< 0.005	0.692 ± 0.066	< 0.005	0.718 ± 0.034	< 0.005	0.644 ± 0.036	< 0.005
DUCKNet	0.638 ± 0.103	< 0.005	0.520 ± 0.092	< 0.005	**0.865 ± 0.047**	< 0.005	0.598 ± 0.108	< 0.005	0.638 ± 0.103	< 0.005

[10] Bui et al. "Meganet: Multi-scale edge-guided attention network for weak boundary polyp segmentation." Proceedings of the IEEE/CVF Winter Conference on Applications of Computer Vision. 2024.
[11] Xu et al. "Levit-unet: Make faster encoders with transformer for medical image segmentation." Chinese Conference on Pattern Recognition and Computer Vision (PRCV). Singapore: Springer Nature Singapore, 2023.
[12] Dumitru et al. "Using DUCK-Net for polyp image segmentation." Scientific reports 13.1 (2023): 9803.

Experimental Results

In-depth Analysis

- The proposed model achieves segmentation accuracy close to the ground truth, surpassing three comparison models. In contrast, comparison models often segment non-target areas or fail to produce results.
- The previous Extraocular muscles segmentation showed good performance in the 2D model on a whole basis and in the 3D model on a single slice basis. This can be found in Common Drawback of Appendix.

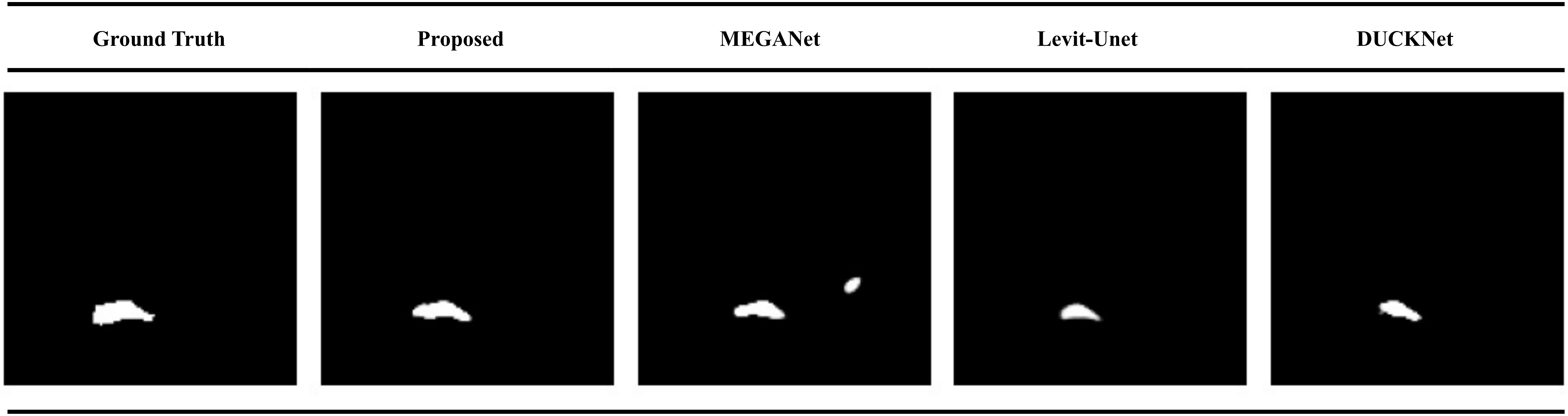

Prediction mask results for each model in comparison with the Ground Truth

Experimental Results

In-depth Analysis

Ablation study

- The Proposed block was compared to the Residual Bottleneck, Split Attention (SA), and Compact Split Attention (CSA) blocks to evaluate its capability, achieving the highest average Dice score.
- Medical images vary widely, requiring data augmentation due to limited datasets. The Proposed block effectively handles diverse resizing ratios through pyramid convolutions with different kernel sizes.

Superiority of Proposed block

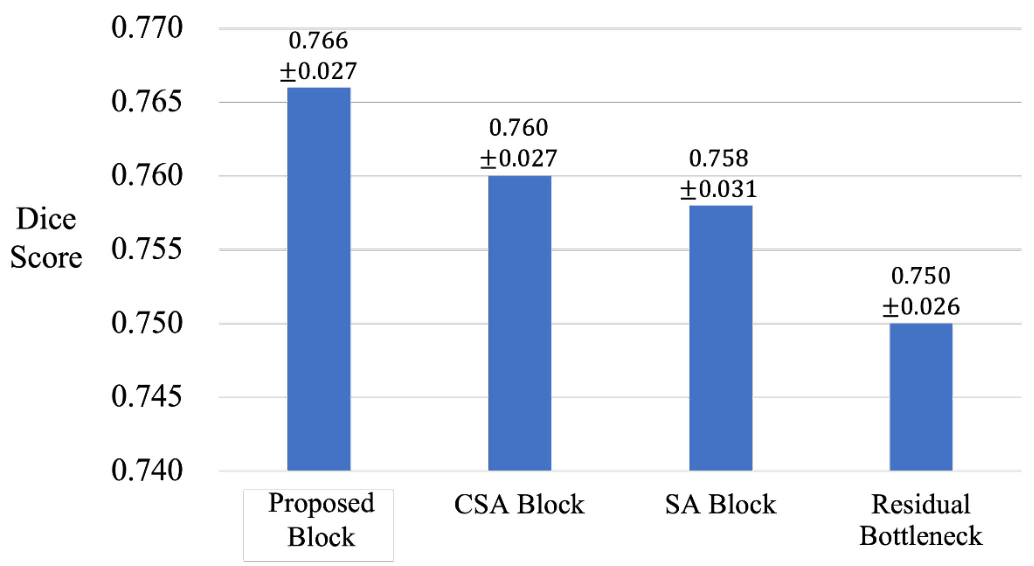

Proposed block for Crop and Resizing augmentation

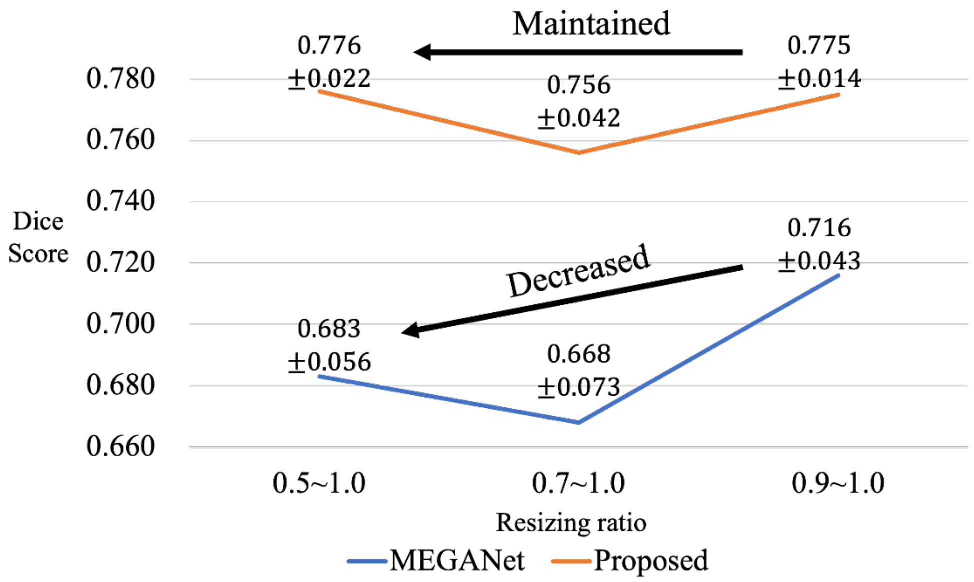

Conclusion and Contribution

- The segmentation performance was improved for the difficult Posterior Extraocular muscles in Orbital apex, which have unclear boundaries and are too small in size.
- We proposed a new neural network that has an effective encoding process for tiny receptive fields to accurately segment small-sized tissues.
- The proposed model demonstrated the highest performance compared to other counterpart models when evaluated on a dataset of 205 TAO patients and significantly better than prior.

Contribution

- Conferences
  - Performance comparison of encoder-decoder for orbit tissue segmentation in CT images, ***IEIE***, 2023
  - A Simple Localization and Classification Framework Based on Template Matching and Self-Attention for TAO Treatment Diagnosis, ***ICCE***, 2024
- Other
  - Medical Technology for Patients with Thyroid-associated Ophthalmopathy, AI Technology-based Employment and Start-up Workshop, 2023, 3rd Prize
  - Internship (AI Researcher/Multimodal AI Image Generation), ***NCSoft***, Seongnam, Korea (2023.09 – 2024.02)

Thank you

Reference

[1] X. Huang et al. "The significance of ophthalmological features in diagnosis of thyroid-associated ophthalmopathy." BioMedical Engineering OnLine 22.1 (2023): 7.

[2] K. Rana et al. "Extraocular muscle enlargement in dysthyroid optic neuropathy." Canadian Journal of Ophthalmology (2023).

[3] Y. Tu et al. "Modified endoscopic transnasal orbital apex decompression in dysthyroid optic neuropathy." *Eye and Vision* 8.1 (2021): 19.

[4] L. Luo et al. "Retinal nerve fiber layer and ganglion cell complex thickness as a diagnostic tool in early stage dysthyroid optic neuropathy." *European Journal of Ophthalmology* 32.5 (2022): 3082-3091.

[5] C.Song et al. "Extraocular muscle volume index at the orbital apex with optic neuritis: a combined parameter for diagnosis of dysthyroid optic neuropathy." European Radiology 33.12 (2023): 9203-9212.

[6] D. Rootman et al. "Orbital decompression for thyroid eye disease." Survey of Ophthalmology 63.1 (2018): 86-104.

[7] J. Diao et al. "Research progress and application of artificial intelligence in thyroid associated ophthalmopathy." *Frontiers in Cell and Developmental Biology* 11 (2023): 1124775.

[8] R. Wang et al. "Medical image segmentation using deep learning: A survey." IET image processing 16.5 (2022): 1243-1267.

[9] F, Yuan et al. "An effective CNN and Transformer complementary network for medical image segmentation." Pattern Recognition 136 (2023): 109228.

[10] N. T. Bui et al. "Meganet: Multi-scale edge-guided attention network for weak boundary polyp segmentation." Proceedings of the IEEE/CVF Winter Conference on Applications of Computer Vision. 2024.

[11] G. Xu et al. "Levit-unet: Make faster encoders with transformer for medical image segmentation." Chinese Conference on Pattern Recognition and Computer Vision (PRCV). Singapore: Springer Nature Singapore, 2023.

[12] R. G. Dumitru et al. "Using DUCK-Net for polyp image segmentation." Scientific reports 13.1 (2023): 9803.

[13] H. Zhang et al. “ResNeSt: Split-Attention Networks.” in *Proceedings of the IEEE/CVF Conference on Computer Vision and Pattern Recognition* 2022.

Appendix

Common Drawback of Conventional Methods

- Best Model
  - Slice : UNETR++
  - Whole : OTSNet
- Best case & Worst case
  - Based on the metric results of patients in the test set, the patients with the highest iou and dice values were designated as best, and the opposite was designated as worst.
- Examples of Visualization

Original	OTSNet	SVNet_2021	SVNet_2023	UNETR++	MEGANet	DUCKNet	Levit-Unet

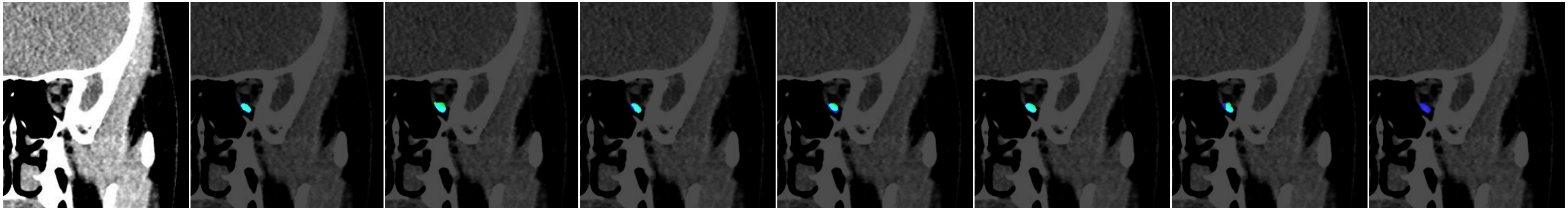

Appendix

Common Drawback of Conventional Methods – Best case (UNETR++)

Slice No.	Original	UNETR++ IoU_slice : 0.793	SVNet_2021 IoU_slice : 0.784	SVNet_2023 IoU_slice : 0.794	OTSNet IoU_slice : 0.795	MEGANet IoU_slice : 0.805	DUCKNet IoU_slice : 0.799	Levit-Unet IoU_slice : 0.715
6								
7								
8								

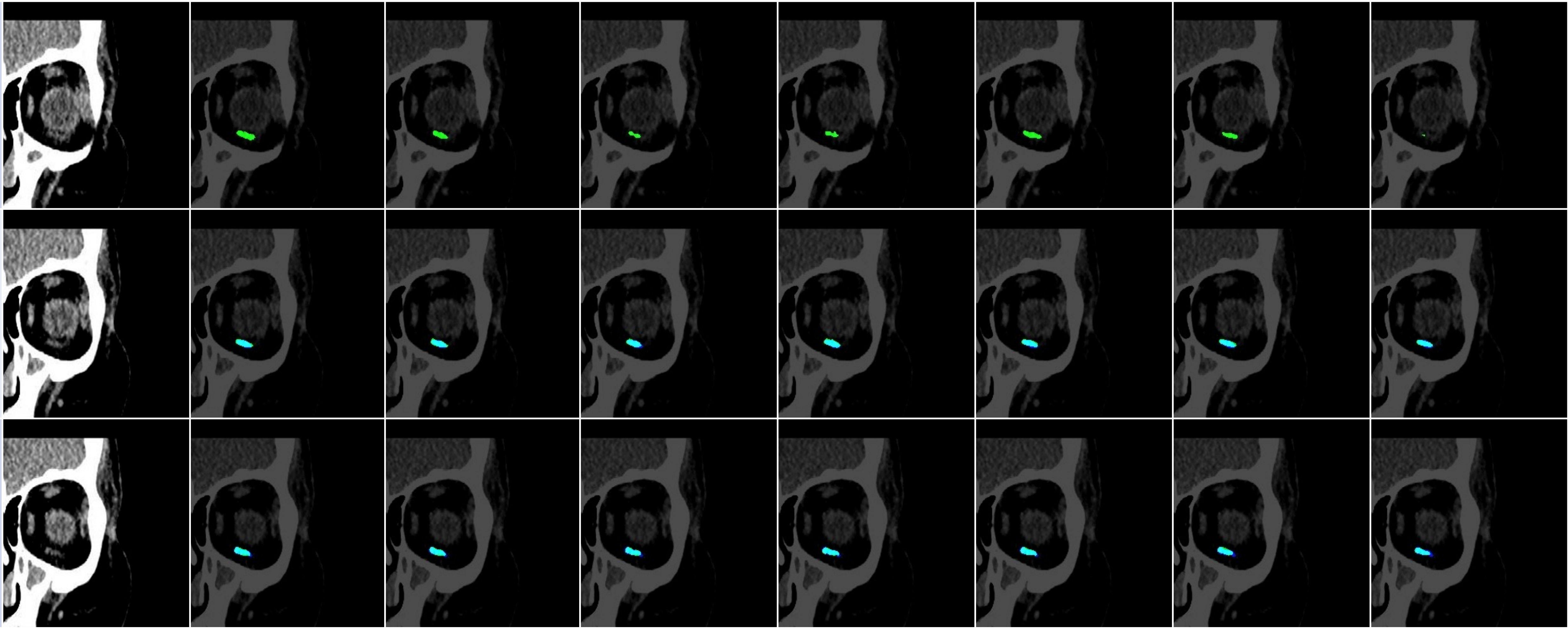

: Ground Truth : Predicted result : Intersection of Ground Truth and Predicted result

Appendix
Common Drawback of Conventional Methods – Best case (UNETR++)

Slice No.	Original	UNETR++ IoU_slice : 0.793	SVNet_2021 IoU_slice : 0.784	SVNet_2023 IoU_slice : 0.794	OTSNet IoU_slice : 0.795	MEGANet IoU_slice : 0.805	DUCKNet IoU_slice : 0.799	Levit-Unet IoU_slice : 0.715
17	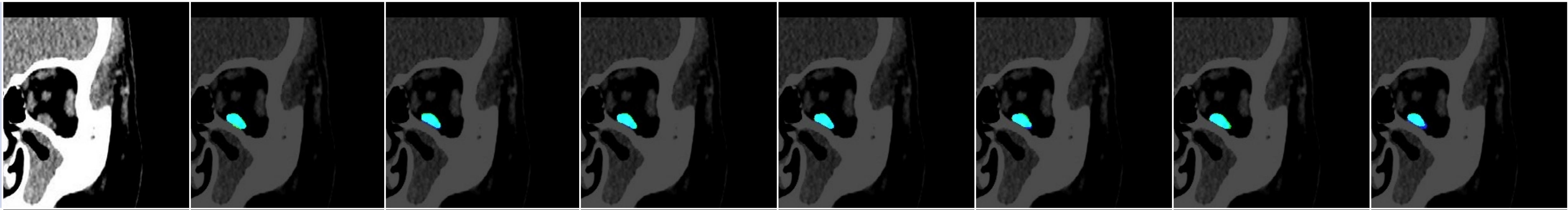							
18	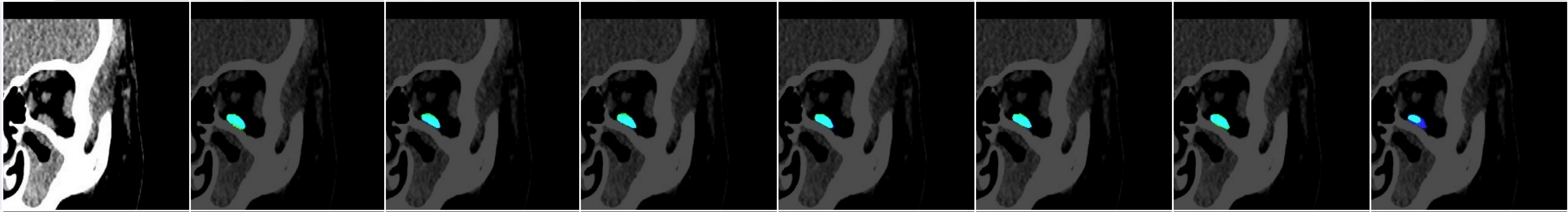							
19	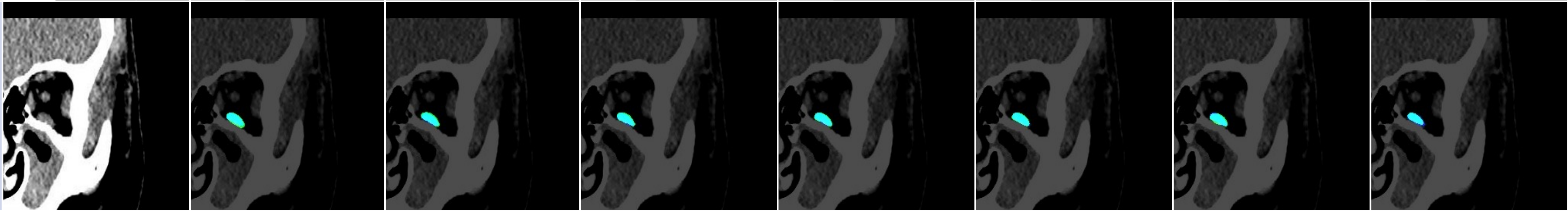							

: Ground Truth : Predicted result : Intersection of Ground Truth and Predicted result

Appendix
Common Drawback of Conventional Methods – Best case (UNETR++)

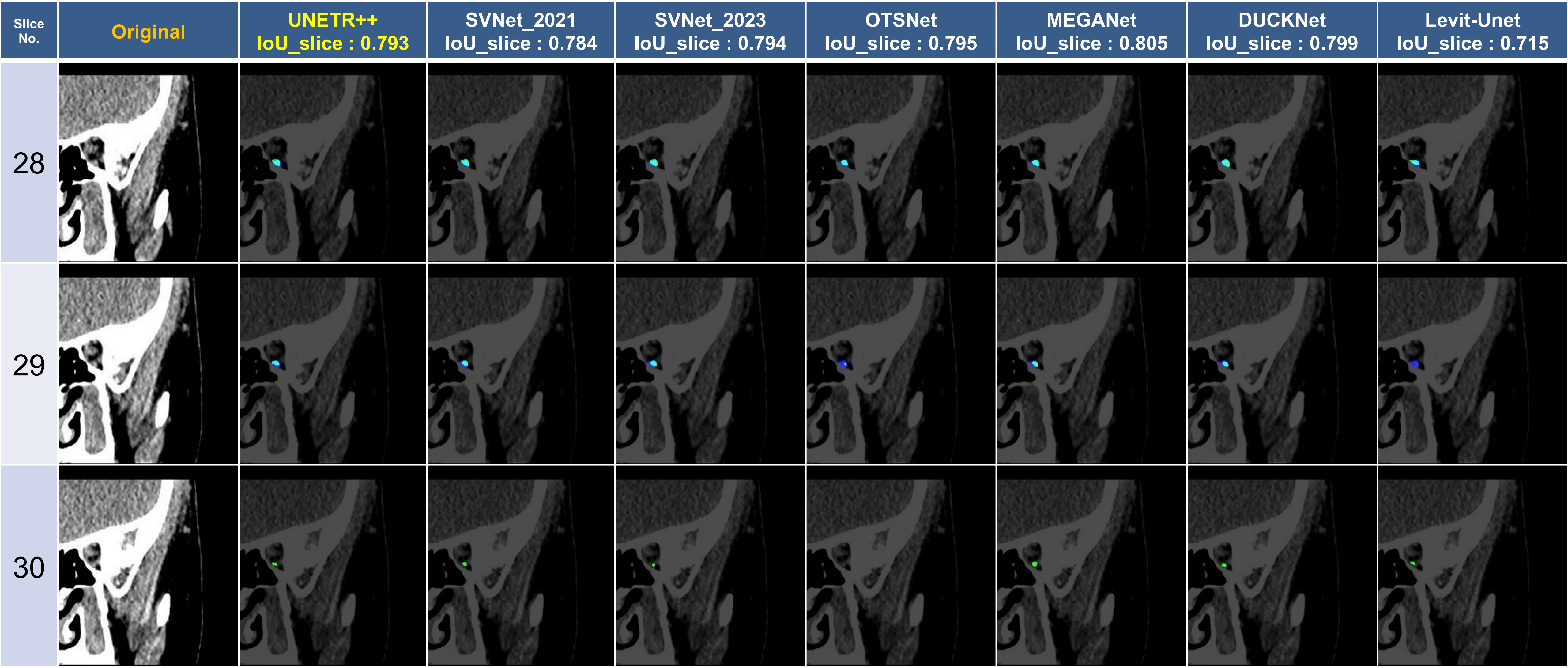

: Ground Truth : Predicted result : Intersection of Ground Truth and Predicted result

Appendix

Common Drawback of Conventional Methods – Worst case (UNETR++)

Slice No.	Original	UNETR++ IoU_slice : 0.512	SVNet_2021 IoU_slice : 0.489	SVNet_2023 IoU_slice : 0.275	OTSNet IoU_slice : 0.470	MEGANet IoU_slice : 0.527	DUCKNet IoU_slice : 0.523	Levit-Unet IoU_slice : 0.502
11	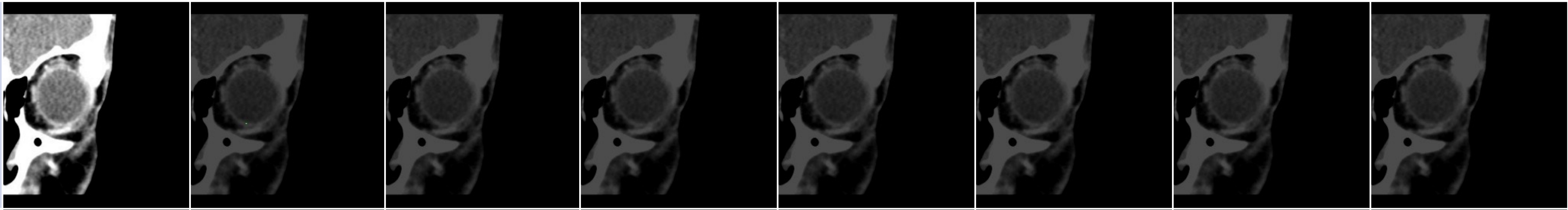							
12	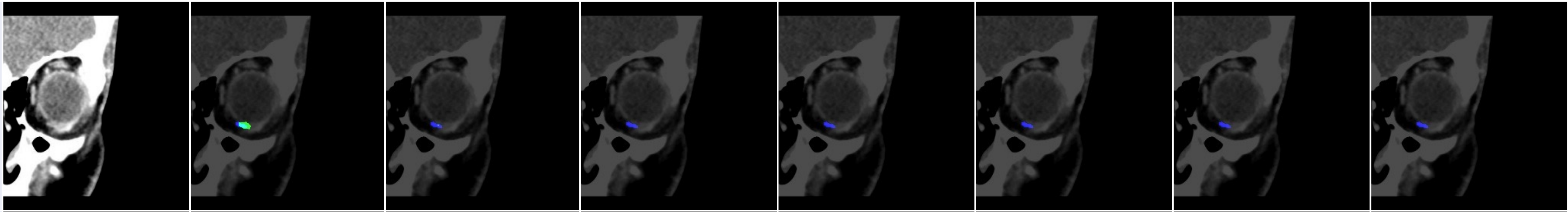							
13	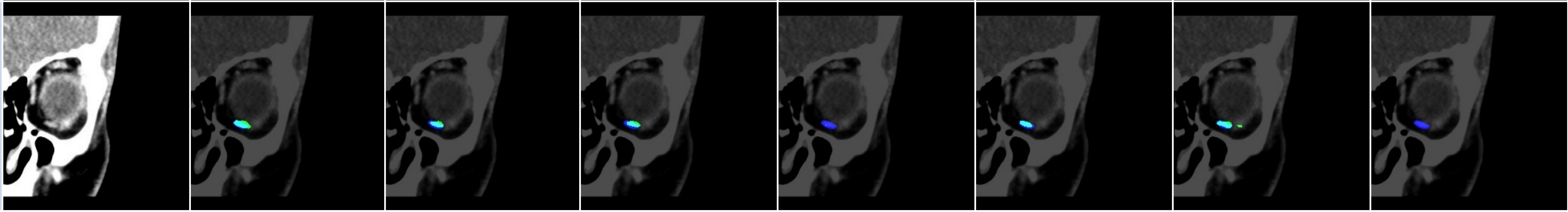							

: Ground Truth : Predicted result : Intersection of Ground Truth and Predicted result

Appendix

Common Drawback of Conventional Methods – Worst case (UNETR++)

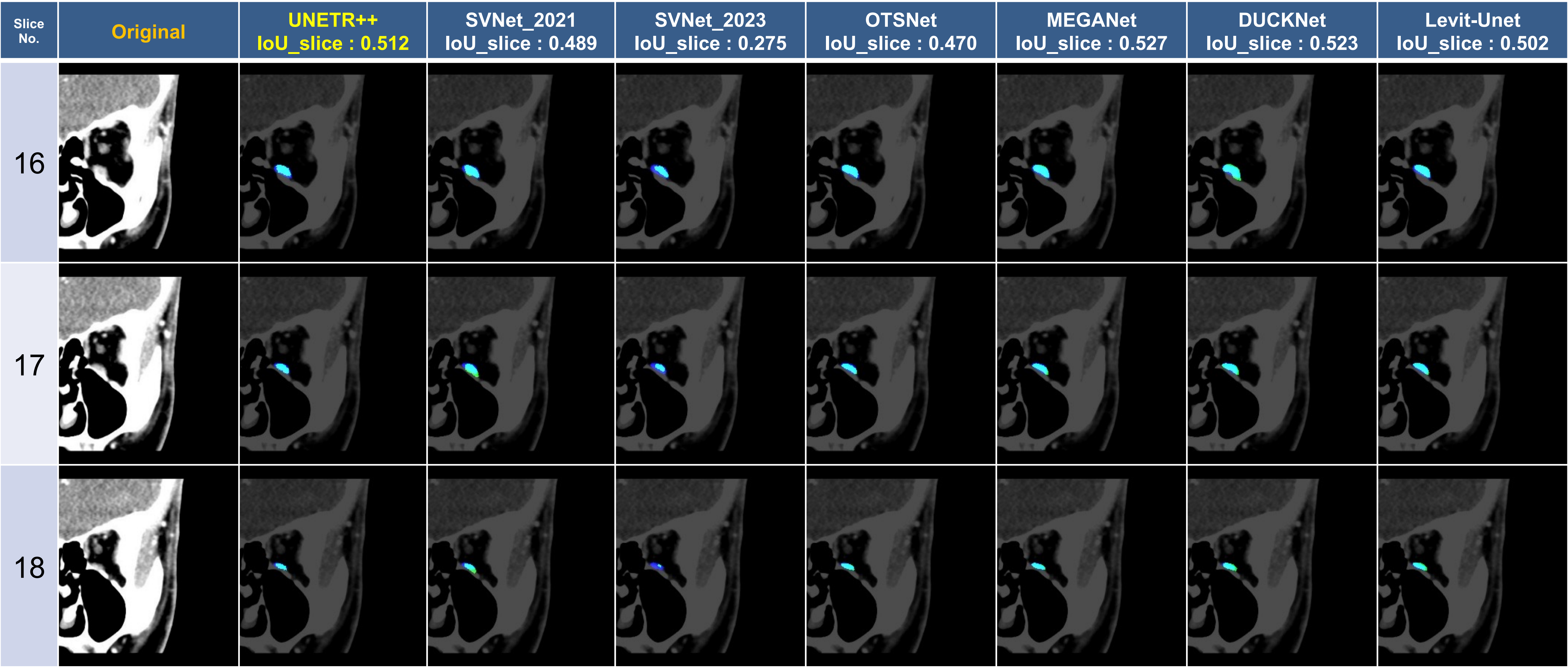

: Ground Truth : Predicted result : Intersection of Ground Truth and Predicted result

Appendix
Common Drawback of Conventional Methods – Worst case (UNETR++)

Slice No.	Original	UNETR++ IoU_slice : 0.512	SVNet_2021 IoU_slice : 0.489	SVNet_2023 IoU_slice : 0.275	OTSNet IoU_slice : 0.470	MEGANet IoU_slice : 0.527	DUCKNet IoU_slice : 0.523	Levit-Unet IoU_slice : 0.502
22								
23								
24								

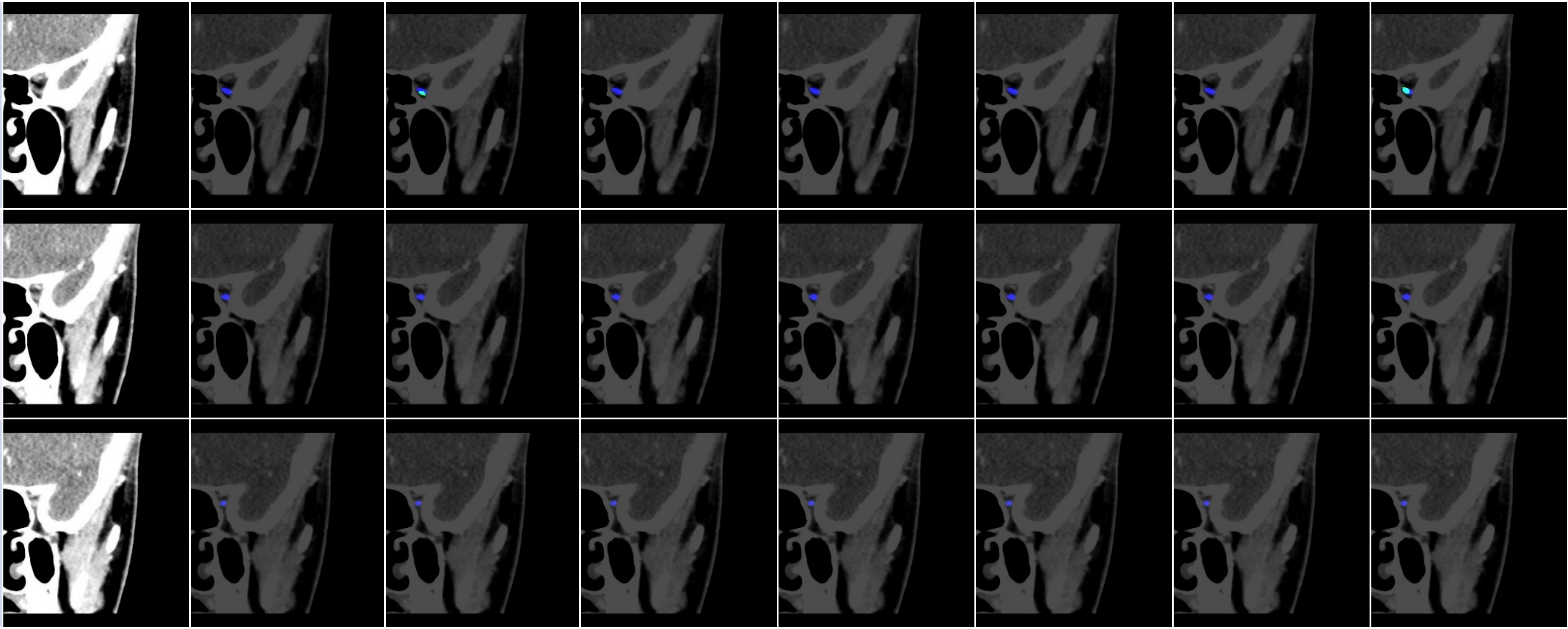

: Ground Truth : Predicted result : Intersection of Ground Truth and Predicted result

Appendix
Common Drawback of Conventional Methods – Best case (OTSNet)

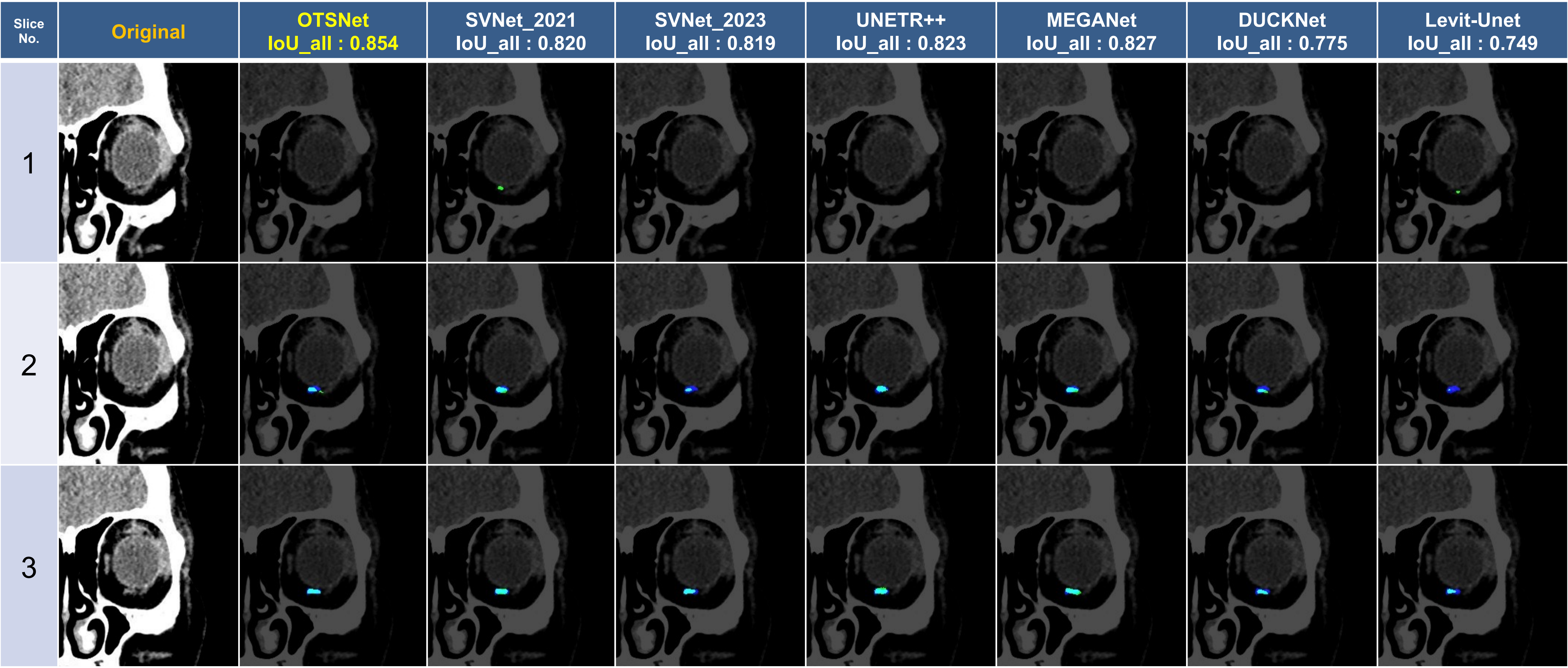

: Ground Truth   : Predicted result   : Intersection of Ground Truth and Predicted result

Appendix
Common Drawback of Conventional Methods – Best case (OTSNet)

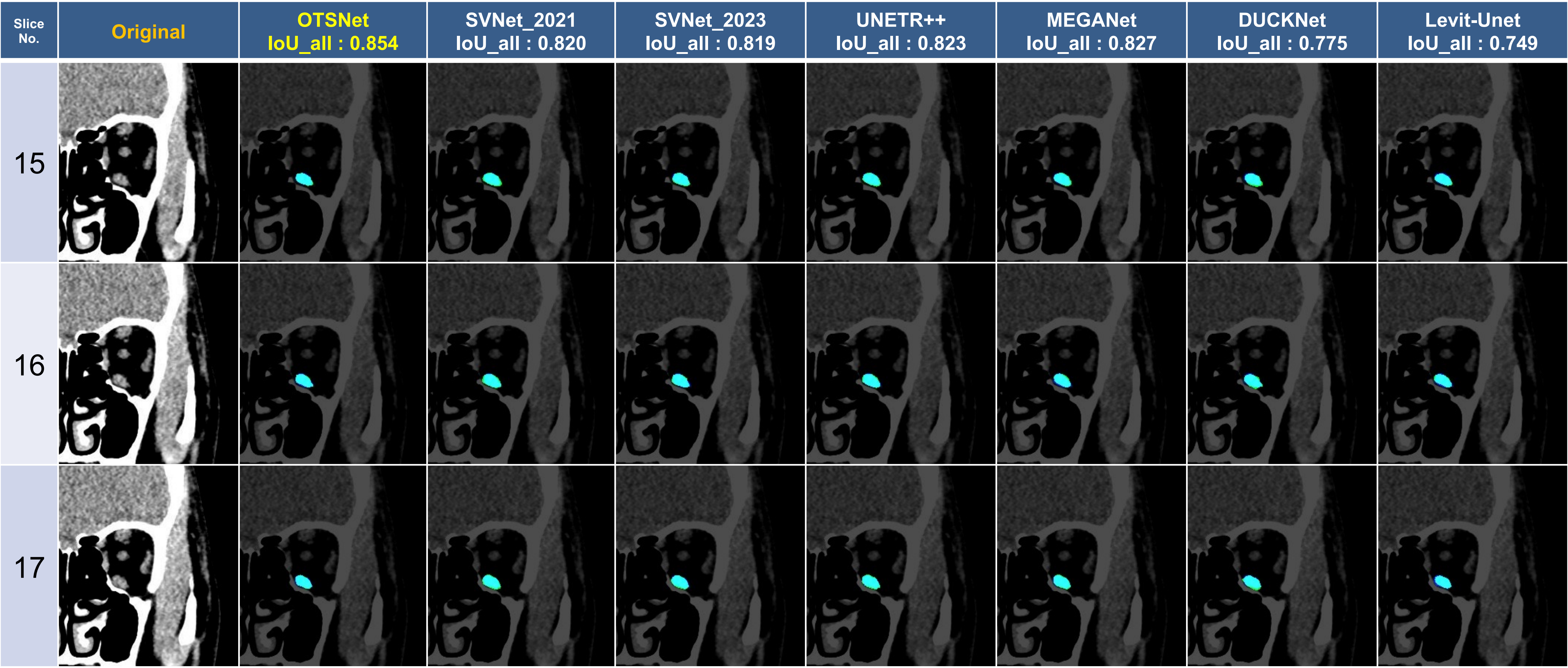

: Ground Truth : Predicted result : Intersection of Ground Truth and Predicted result

Appendix

Common Drawback of Conventional Methods – Best case (OTSNet)

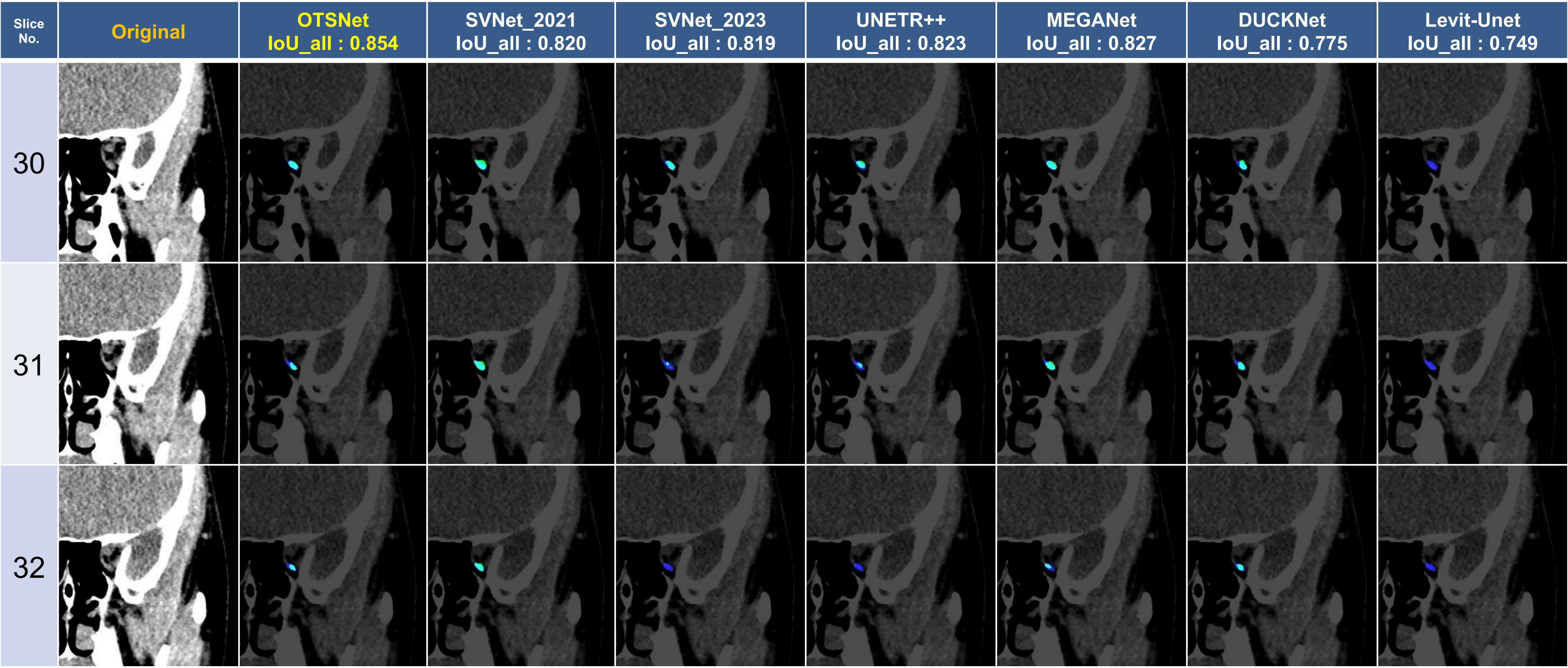

: Ground Truth : Predicted result : Intersection of Ground Truth and Predicted result

Appendix

Common Drawback of Conventional Methods – Worst case (OTSNet)

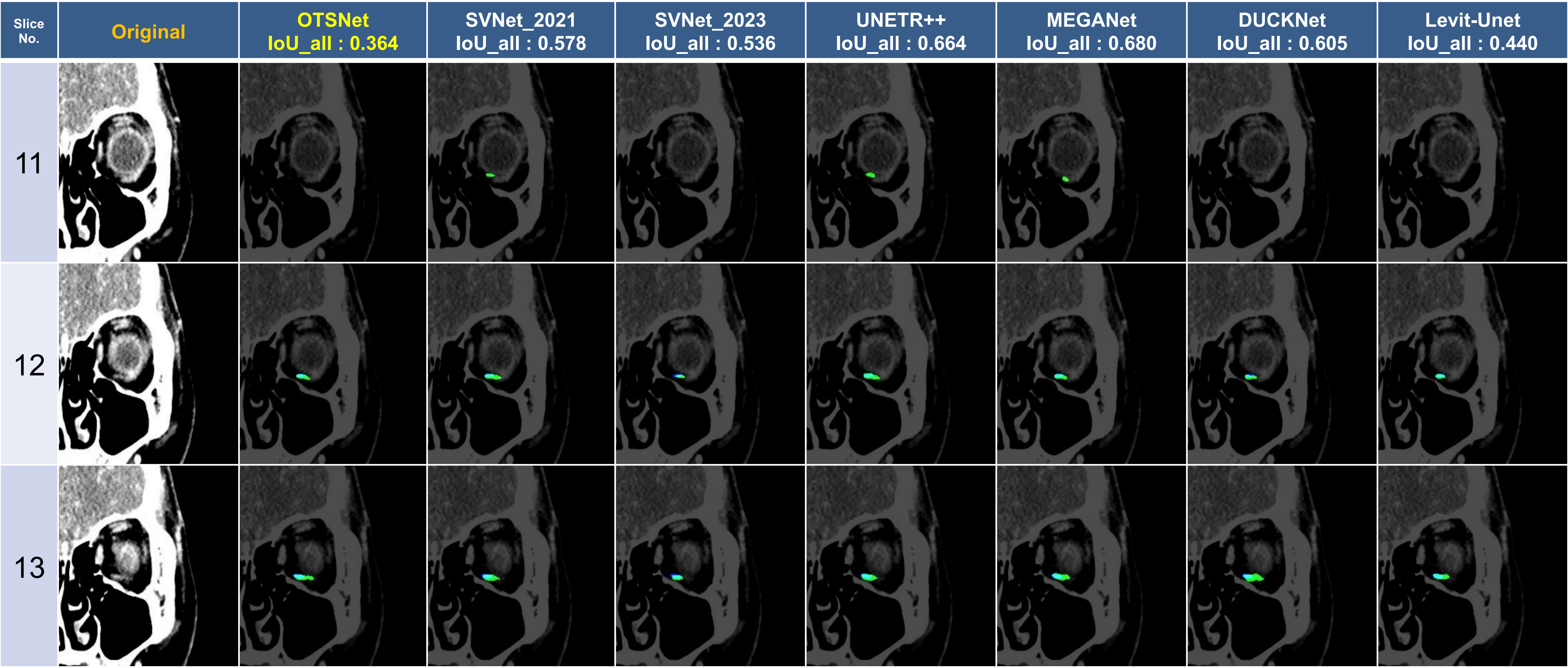

: Ground Truth   : Predicted result   : Intersection of Ground Truth and Predicted result

Appendix

Common Drawback of Conventional Methods – Worst case (OTSNet)

Slice No.	Original	OTSNet IoU_all : 0.364	SVNet_2021 IoU_all : 0.578	SVNet_2023 IoU_all : 0.536	UNETR++ IoU_all : 0.664	MEGANet IoU_all : 0.680	DUCKNet IoU_all : 0.605	Levit-Unet IoU_all : 0.440
16								
17								
18								

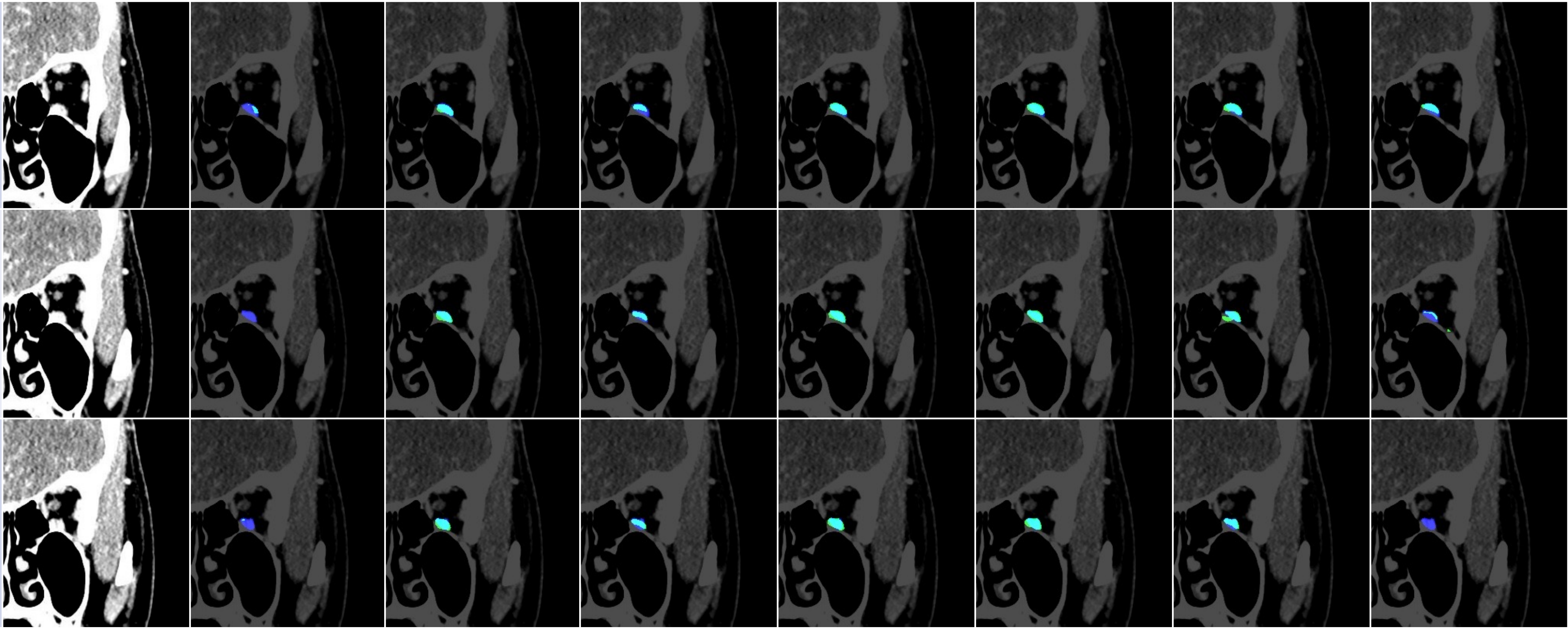

: Ground Truth : Predicted result : Intersection of Ground Truth and Predicted result

Appendix
Common Drawback of Conventional Methods – Worst case (OTSNet)

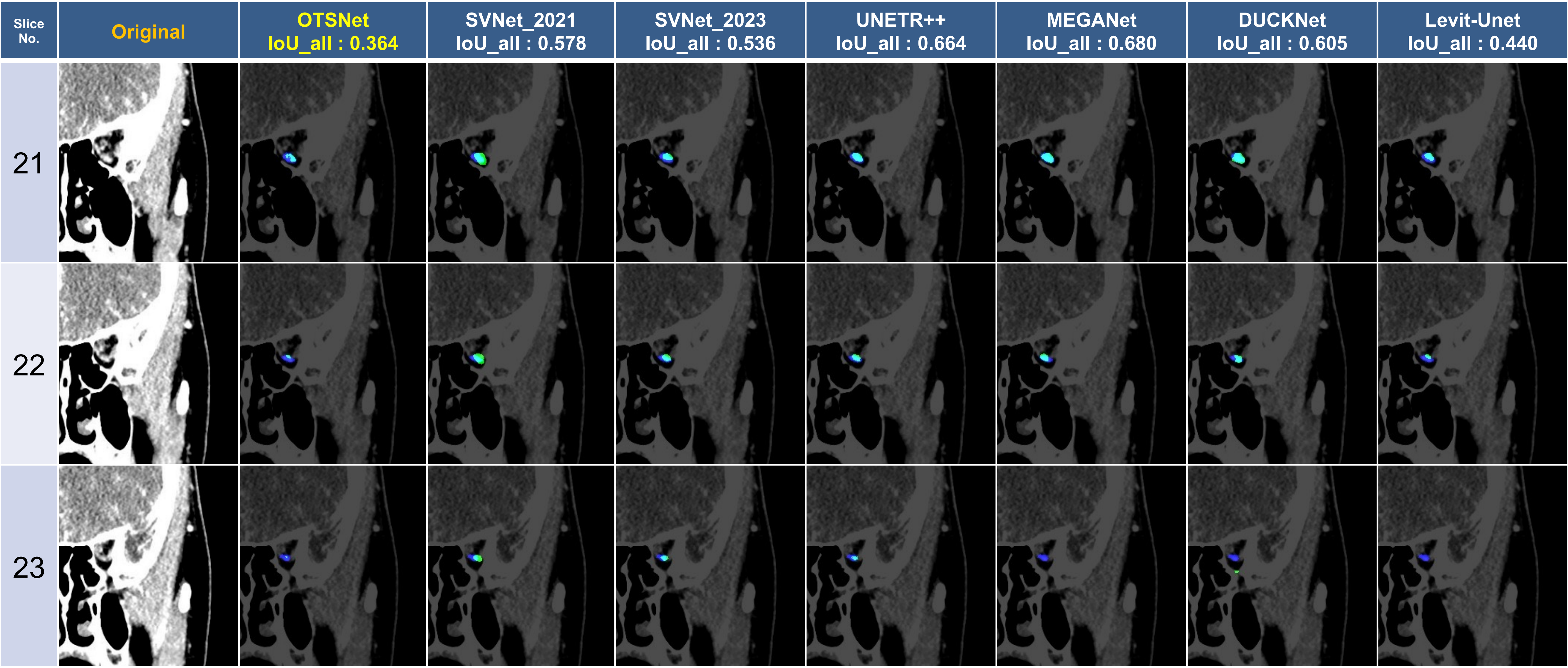

: Ground Truth : Predicted result : Intersection of Ground Truth and Predicted result